Appendix M

Cosine Curves of Simulated Circular Random Fields (CRF)

M.1 Review

This appendix characterizes the circular-spatial correlation produced by the method of simulating CRFs of Chapter 5. This form of circular-spatial correlation is expressed as the mean cosine of the angle between random components of directions vs. distance between observation locations, which is required to solve the kriging of circular RV of Chapter 4. Since the method involves transformations of the nonclosed form of the normal CDF and a circular inverse CDFs, some of which do not have closed form expression, exact expressions for the cosine curves were not derived. Instead, the cosine curves produced by the method were characterized by fitted models adapted from the covariance models used for kriging of linear RV. The covariance models with variance 1 were adapted by Equation (5.2) in Chapter 5, Subsection 5.4.2.2 to the behavior of the mean cosine of a CRF.

M.2 Generation of Cosine vs. Distance Curves

For characterization of the mean cosine vs. distance of the simulated CRF, cosine vs. distance curves were generated using the R code in Appendices K.14 and L.10. The commands in L.10 specify 126 different sets of simulation inputs based on:

- The cardioid, triangular, uniform, von Mises, and wrapped Cauchy circular probability distributions as described in Table 5-1 in Chapter 5, Section 5.3,
- 5 values of the parameter ρ of a circular probability distribution (See Table M-1),
- Range *r*, the scale parameter of the covariance model of the Gaussian random field (GRF), at 5 and 10, and

Table M-1. Mean Resultant Vector Length ρ of Circular Distributions for Figures M-2, M-3, and M-4.

Index	% of ρ max	Cardioid	Triangular	Uniform	von Mises	Wrapped Cauchy
1	5%	0.025	0.020	0.000	0.050	0.050
2	25%	0.125	0.101		0.250	0.250
3	50%	0.25	0.203		0.500	0.500
4	75%	0.375	0.304		0.750	0.750
5	95%	0.475	0.385		0.950	0.950
	Range of ρ	$0 < \rho \leq 0.5$	$0 < \rho \leq 4/\pi^2$	$\rho = 0$ *	$0 < \rho < 1$	$0 < \rho < 1$

* All directions of the uniform circular distribution have equal probability density resulting in a mean resultant length ρ of zero.

- Exponential, Gaussian, spherical covariance models $c(d)$ of the GRF as listed in Chapter 5, Subsection 5.2.2, step 4).

For each of the 126 sets of inputs, 400 simulations of the CRF were computed without standardization of the GRF (Chapter 5, Section 5.3, step 1). For each simulation, 400 observations of direction at random sample locations were computed, and a cosineogram (Chapter 3) was evaluated.

For each of the 126 sets of inputs, the cosineograms points were collected into a datasets. Each dataset was reduced to a curve of cosine vs. distance by local polynomial regression of degree 1 (Wand and Jones 1995). These curves will be shown in the next section.

Do these curves represent the underlying spatial dependence produced by the method of simulation? Figure M-1 was constructed using the R code in Appendix L, Section L.11. 400 variograms of simulations of a GRF with spherical covariance, range=10, and variance=1, were reduced by local polynomial regression of degree 1 to a curve of variance vs. distance. The variance vs. distance curve was transformed to covariance vs. distance (Bailey and Gatrell 1995, p. 163).

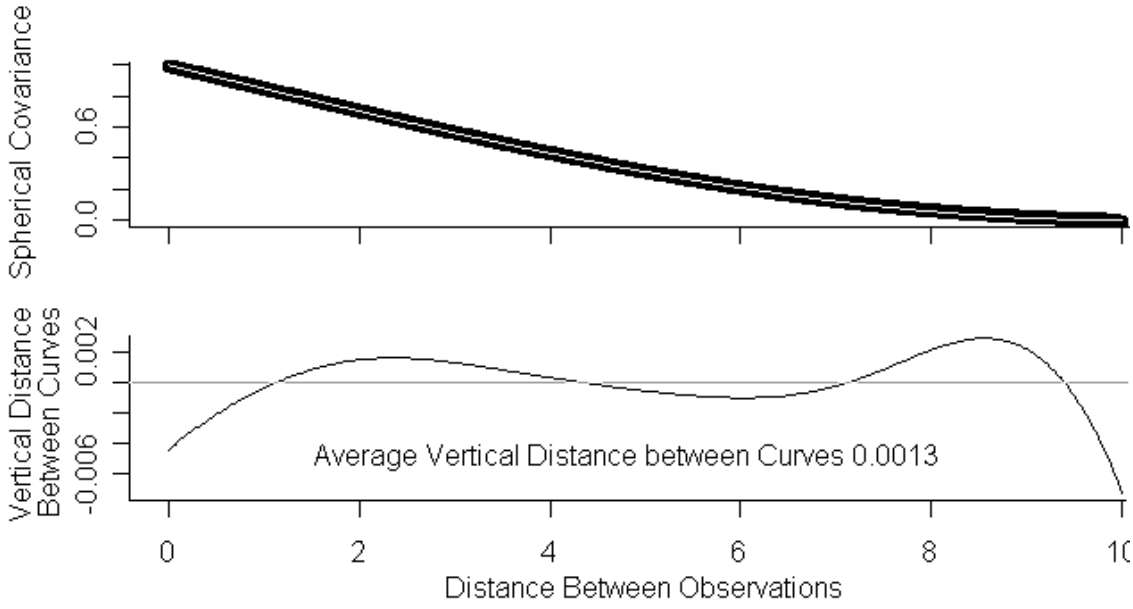

Figure M-1, Fitted Covariogram an Unbiased Estimator of Spherical Covariance

In the top plot, the theoretical covariance is over plotted in white on the covariance curve from the simulations (black). Visually, the curves coincide indicating that the fitted curve is unbiased. The bottom plot shows the difference of the covariance curve minus the theoretical covariance. The average vertical distance between curves is 0.001. Thus, the proximity of the curves provides verification by simulation that the curves in the next section are unbiased estimates of the spatial dependence produced by the method of simulation, and justifies the approach of the next section.

M.3 Families of Cosine Curves

Figures M-2 to M-4, which were constructed using the R code in Appendix L, Section L.12, show 126 curves of the mean cosine vs. distance derived from the data sets. The combinations of ρ and range provide a full spectrum of cosine curves for each input covariance model of the Gaussian random field (GRF). The black curves have range=5 and the tan curves have range=10. ρ increases from (1) to (5) as specified by the values in Table M-1 because the maximum value of ρ depends on the circular probability distribution. Examination of these figures indicates that each GRF covariance model (exponential, Gaussian, spherical) produces a distinct family of CRF cosine curves of similar shape. The exponential covariance model in Figure M-2 produces a cosine curve that approaches a horizontal asymptote as distance increases similar to the exponential covariance model. The Gaussian covariance model in Figure M-3 produces a cosine curve that has an “S” shape similar to the Gaussian covariance model. The spherical covariance model in Figure M-4 produces a cosine curve that has a horizontal tangent at distance=range similar to the spherical covariance model.

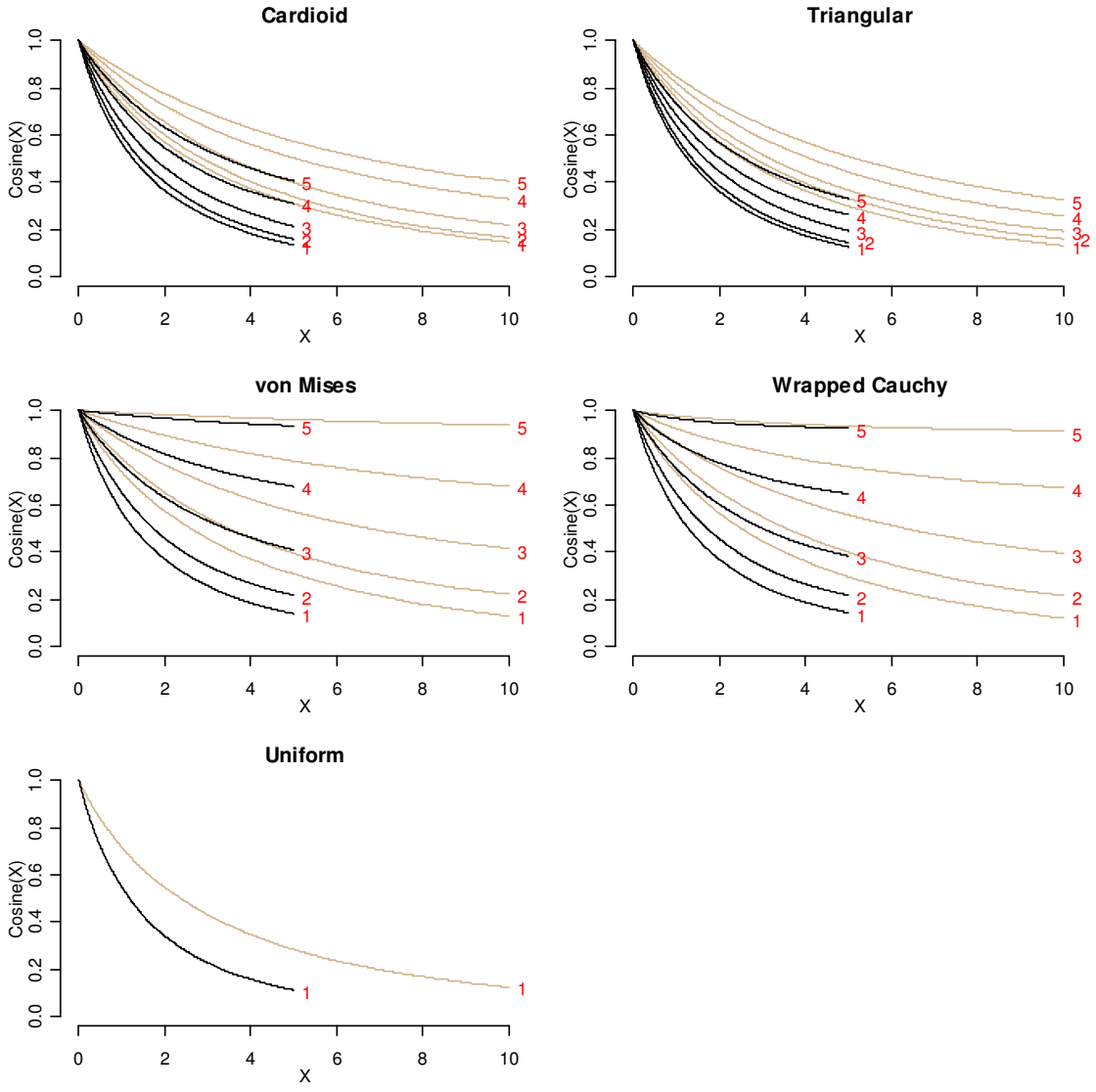

Figure M-2. Family of Cosine vs. Distance Curves from the GRF with Exponential Covariance. The black curves have range = 5 and the tan curves have range = 10. Within the classes of circular probability distributions and range value, the parameter ρ increases from bottom to top (Cross reference red numbers to Index values in Table M-1). The exponential covariance produces a curve that approaches a horizontal asymptote as distance increases similar to the exponential covariance model.

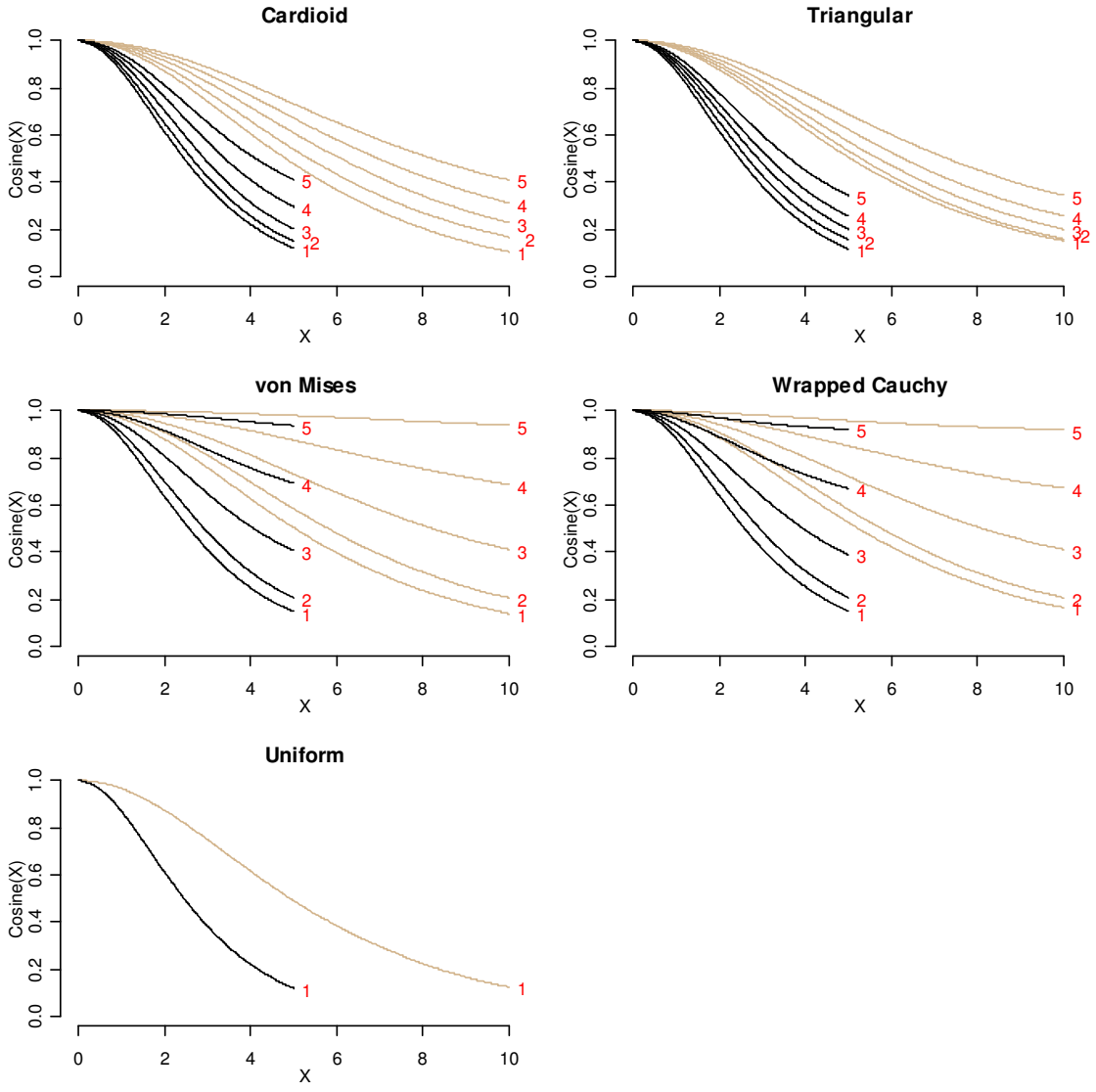

Figure M-3. Family of Cosine vs. Distance Curves from the GRF with Gaussian Covariance. The black curves have range = 5 and the tan curves have range = 10. Within the classes of circular probability distributions and range value, the parameter ρ increases from bottom to top (Cross reference red numbers to Index values in Table M-1). The Gaussian covariance produces a curve that has an "S" shape similar to the Gaussian covariance model.

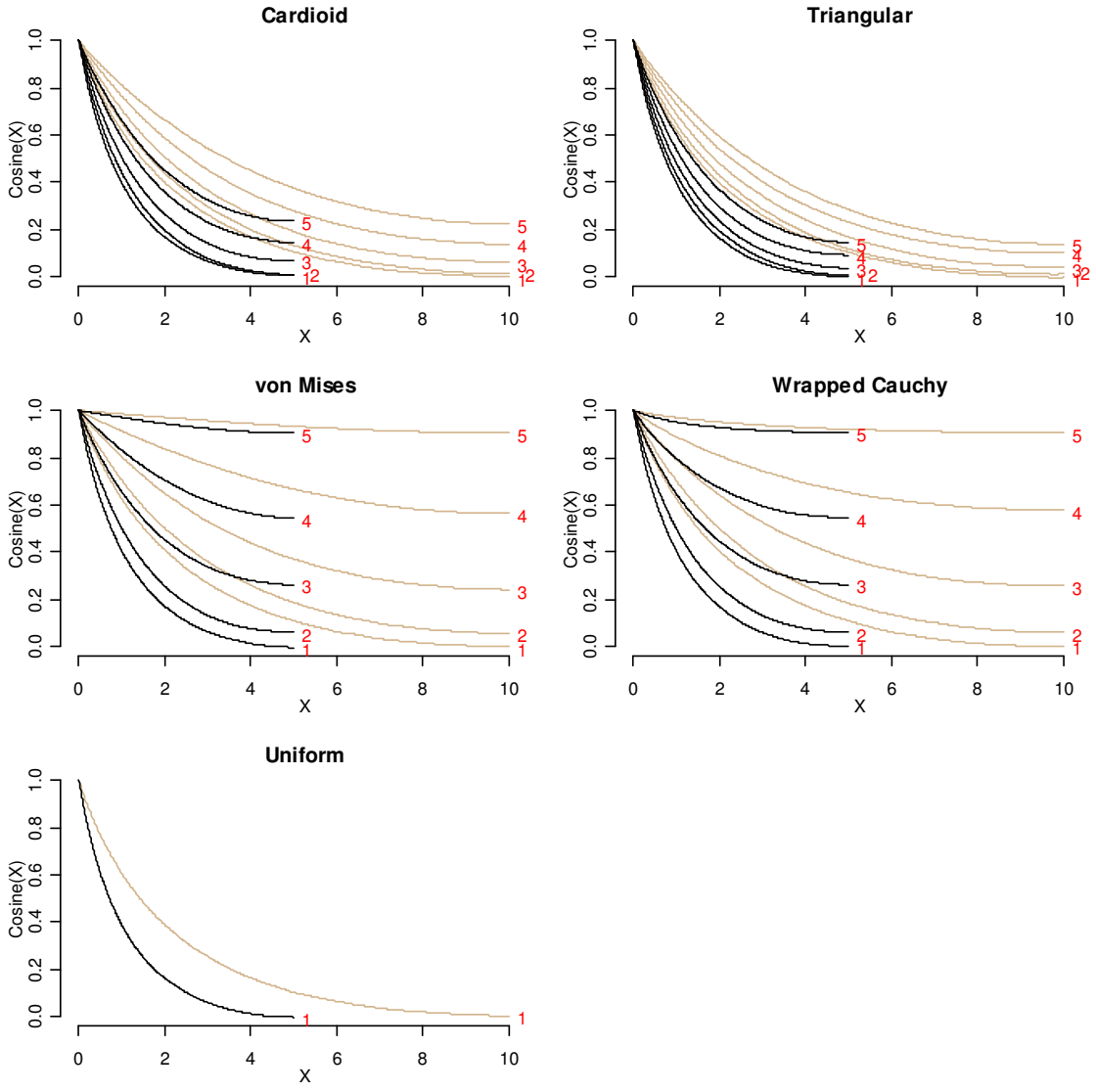

Figure M-4. Family of Cosine vs. Distance Curves from the GRF with Spherical Covariance. The black curves have range = 5 and the tan curves have range = 10. Within the classes of circular probability distributions and range value, the parameter ρ increases from bottom to top (Cross reference red numbers to Index values in Table M-1). The spherical covariance produces a curve that has a horizontal tangent at distance = range similar to the spherical covariance model.

M.4 Characterization of the Cosine Curves

To characterize the cosine curves, covariance models for linear kriging were shifted and scaled to conform to the spatial correlation properties of the CRF. With $\varsigma(d)$ the mean cosine of the angle between random components of direction as a function of distance d, ρ the mean resultant length of the circular probability distribution, $0 \le \rho < 1$, n_g the nugget, $0 \le n_g \le 1-\rho^2$, and $c(d)$ the covariance model with a maximum value of one, the cosine model was defined as

$$\varsigma(d) = \begin{cases} 1, d = 0 \\ \rho^2 + (1 - n_g - \rho^2)c(d), d > 0. \end{cases} \quad \text{(M.1)}$$

A cosine model with shape similar to the cosine curve was chosen. The cosine curve was fit using a plot such as Figure M-5, which was produced using the R code in Appendix K, Section K.15. The lower plot shows the mean absolute difference (MAD) between the cosine curve and cosine model as computed over distances from 0 to the range. The three parameter cosine model was fit as follows: The value of a parameter was changed to determine how to decrease the MAD. Adjustment of the parameter continued until the MAD began to increase. Then, the parameter was changed in the opposite direction at a finer resolution. When a local minimum was achieved, another parameter was adjusted to a local minimum. Next, the third parameter was adjusted to a local minimum. The entire process was repeated with the modification that when a parameter could not be adjusted, adjustment of the next parameter was attempted. When any parameter was adjusted, adjustment of the remaining parameters was attempted. When no further adjustment could be made, the parameters and the MAD were recorded.

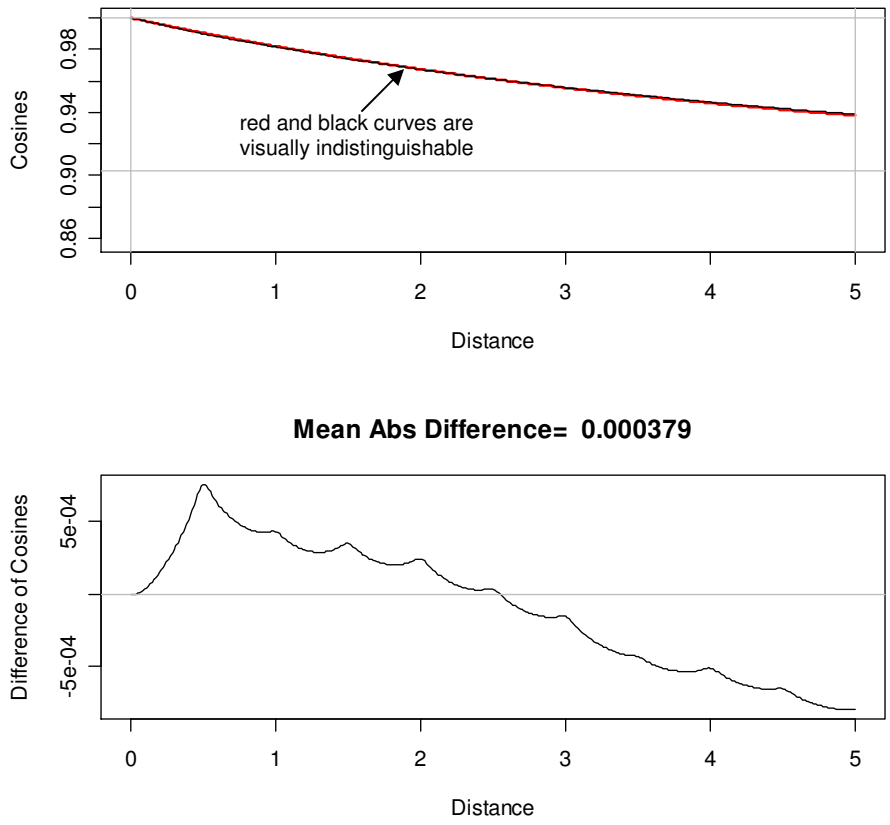

Figure M-5. Whittlematern Cosine Model (a=.493) Approximates the Cosine Curve of the von Mises CRF, $\rho = 0.95$, Transformed from an Exponential GRF, Range $r = 5$.

The characterizing models of reasonably close fit are tabulated in Table M-2. The input GRF covariance models are listed in the top rows of the sub tables. The dataset names in the left margin code the other simulation inputs of the distribution {Uniform (U), Cardioid (card), Triangular (tri), von Mises (vM), Wrapped Cauchy (WrC)}, the parameter ρ {.05, .95}, and the range r {5, 10}. The second row of the sub tables lists the characterizing models, which are expressed in Section M.5. In the main part of the table, the cosine model parameter values are listed in order a, b, c. Where fit was not reasonably close, additional models were evaluated. Where more than one model fits a cosine curve, the model with the minimum MAD may be chosen.

Table M-2. Cosine Models Approximating CRF Cosine Curves.

Cosine Models	Gaussian GRF							
	cauchytbm a in (0,2] b > 0, c >1		gencauchy a in (0,2] b > 0		hyperbolic a > 0, b > 0, c >= 0, or a > 0, b = 0, c > 0, or a >= 0, b < 0, c > 0		stable a in (0,2]	
	Parameters	MAD	Parameters	MAD	Parameters	MAD	Parameters	MAD
card.05.5	1.80, 2.90, 2.40	0.005	1.84, 5.39	0.004				
card.05.10	1.80, 2.85, 2.40	0.016	1.84, 5.60	0.007				
card.95.5	2.00, 1.60, 1.45	0.004	2.00, 3.93	0.004				
card.95.10	2.00, 1.58, 1.37	0.004	2.00, 3.92	0.005				
tri.05.5	1.84, 2.97, 2.40	0.003	1.85, 5.40	0.005				
tri.05.10	1.80, 2.68, 2.19	0.008	1.83, 5.02	0.002				
tri.95.5	2.00, 1.96, 1.80	0.001	2.00, 4.16	0.003				
tri.95.10	2.00, 1.94, 1.80	0.001	2.00, 4.13	0.002				
U.5	1.83, 2.65, 2.29	0.002	1.85, 5.47	0.003				
U.10	1.84, 2.85, 2.23	0.002	1.85, 5.40	0.003				
vM.05.5	1.80, 2.55, 2.10	0.004	1.86, 5.12	0.002				
vM.05.10	1.82, 2.71, 2.20	0.003	1.90, 5.50	0.002				
vM.95.5	fit not close	-	fit not close	-			1.95	0.001
vM.95.10	fit not close	-	fit not close	-	7.45, 0.00, 3.30	0.002		
WrC.05.5	1.86, 2.75, 2.32	0.002	1.90, 5.26	0.002				
WrC.05.10	1.86, 2.69, 2.33	0.003	1.90, 5.11	0.003				
WrC.95.5	1.90, 2.60, 2.20	0.001	1.91, 4.78	0.0003				
WrC.95.10	1.70, 2.60, 3.68	0.002	fit not close	-	0.50, -0.72, 0.47	0.002		

Cosine Models	Exponential GRF						Spherical GRF	
	cauchytbm a in (0,2] b > 0, c >= 1		gencauchy a in (0,2] b > 0		whittlematern a > 0		cauchytbm a in (0,2] b > 0, c >= 1	
	Parameters	MAD	Parameters	MAD	Parameters	MAD	Parameters	MAD
card.05.5	0.90, 1.29, 1.00	0.002	0.95, 2.74	0.002			0.96, 2.42, 1.19	0.003
card.05.10	0.92, 1.35, 1.12	0.003	0.94, 2.65	0.003			0.97, 2.45, 1.19	0.002
card.95.5	1.02, 1.01, 1.01	0.006	1.03, 2.05	0.005			1.16, 2.12, 1.07	0.005
card.95.10	1.05, 1.05, 1.01	0.003	1.09, 2.29	0.003			1.17, 2.07, 1.00	0.006
tri.05.5	0.88, 1.27, 1.00	0.008	0.92, 2.64	0.006			0.98, 2.52, 1.20	0.002
tri.05.10	0.92, 1.51, 1.30	0.002	0.92, 2.60	0.005			1.00, 2.70, 1.29	0.003
tri.95.5	1.02, 1.09, 1.02	0.003	1.04, 2.28	0.002			1.13, 2.11, 1.00	0.005
tri.95.10	1.02, 1.08, 1.02	0.005	1.04, 2.28	0.003			1.14, 2.25, 1.04	0.005
U.5	0.93, 1.57, 1.24	0.002	0.93, 2.84	0.005			0.94, 2.24, 1.07	0.003
U.10	0.91, 1.34, 1.00	0.003	0.96, 2.92	0.004			0.98, 2.67, 1.31	0.002
vM.05.5	0.95, 1.55, 1.33	0.002	0.96, 2.76	0.001			0.97, 230, 1.09	0.003
vM.05.10	0.95, 1.55, 1.32	0.002	0.96, 2.77	0.003			0.98, 2.45, 1.18	0.003
vM.95.5	fit not close	-	fit not close	-	0.46	0.0009	1.42, 1.99, 1.00	0.001
vM.95.10	fit not close	-	fit not close	-	0.48	0.0003	1.42, 2.00, 1.00	0.001
WrC.05.5	0.93, 1.56, 1.40	0.002	0.93, 2.63	0.002			0.99, 2.55, 1.21	0.003
WrC.05.10	0.93, 1.52, 1.26	0.003	0.93, 2.71	0.006			0.98, 2.48, 1.20	0.003
WrC.95.5	0.96, 1.30, 1.47	0.0003	0.97, 2.15	0.0006			1.05, 2.25, 1.22	0.0006
WrC.95.10	0.95, 1.29, 1.00	0.001	0.99, 2.80	0.001			1.07, 2.26, 1.19	0.0008

M.5 Expressions for the Cosine Models of Table M-2

The models in Table M-2, which approximate the cosine curves, and hence characterize them, were adapted from R package RandomFields (Schlather 2001) function CovarianceFct by scaling and shifting (Chapter 5, Subsection 5.4.2.2, (5.2)). In this section, these cosine models $\varsigma(x)$ will be simplified by assuming the nugget $n_g = 0$, and expressed in terms of distance *d*, range *r*, $x = d/r$, ρ the resultant mean length parameter of the circular probability distribution, $0 \le \rho < 1$, and covariance parameters a, b, and c. Figures M-6 to M-10 were computed using the R code in Appendix L, Section L.13.

M.5.1 Whittlematern:

$$\varsigma(x) = \rho^2 + \left(1 - \rho^2\right)\frac{2^{(1-a)}}{\Gamma(a)}\, x^a\, K_a(x),\ a > 0 \qquad \text{(M.2)}$$

$K_a(x)$ denotes the modified Bessel function of the third kind of order *a*.

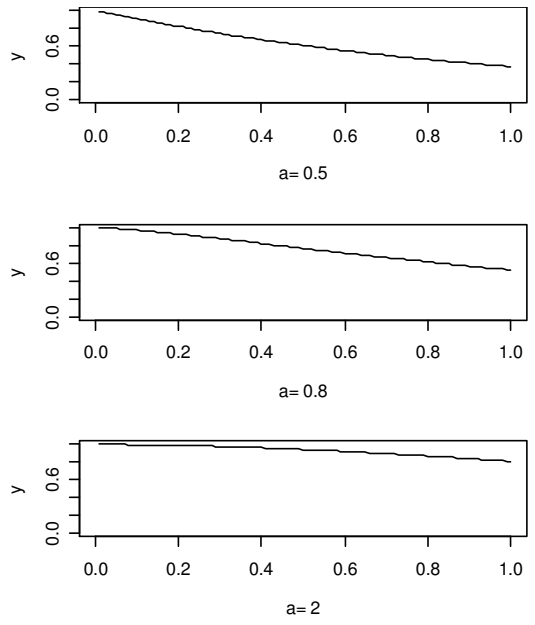

Figure M-6. Whittlematern Cosine Models for $\rho = 0$.

M.5.2 Cauchytbm:

$$\varsigma(x) = \rho^2 + \left(1 - \rho^2\right)\left(1 + \left[1 - b/c\right]x^a\right)\left(1 + x^a\right)^{(-b/a - 1)},\ a \in (0,2],\ b > 0, c \geq 1 \qquad \text{(M.3)}$$

Cauchytbm models are illustrated in Figure M-7 for $\rho = 0$ with parameter c=2 as black solid, c=4 as tan, and c=6 as thick dashed black curves.

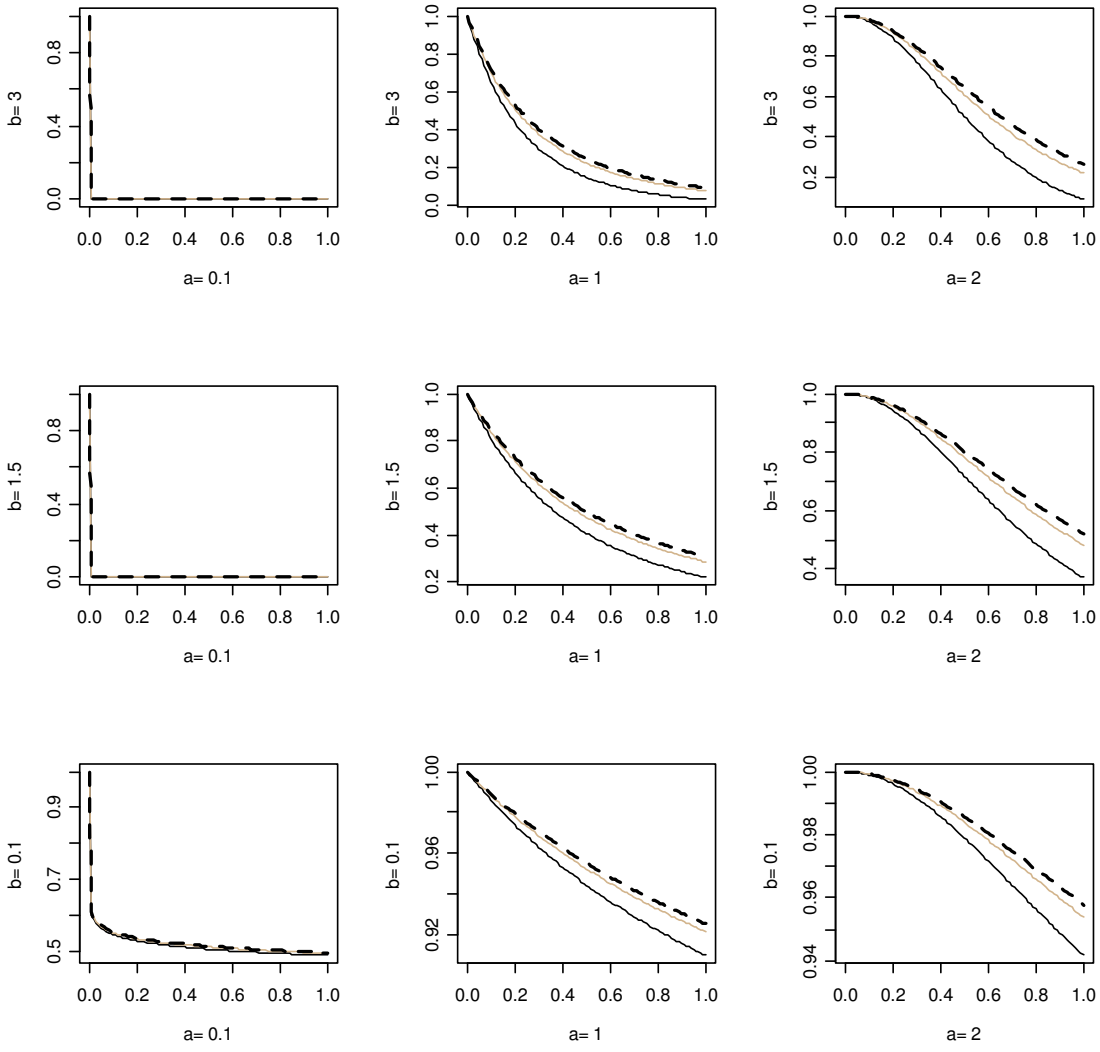

Figure M-7. Cauchytbm Cosine Models for $\rho = 0$.

M.5.3 Generalized Cauchy:

$$\varsigma(x) = \rho^2 + \left(1-\rho^2\right)\left(1+x^a\right)^{-b/a},\ a \in (0,2],\ b > 0 \qquad \text{(M.4)}$$

Generalized Cauchy cosine models are illustrated in Figure M-8.

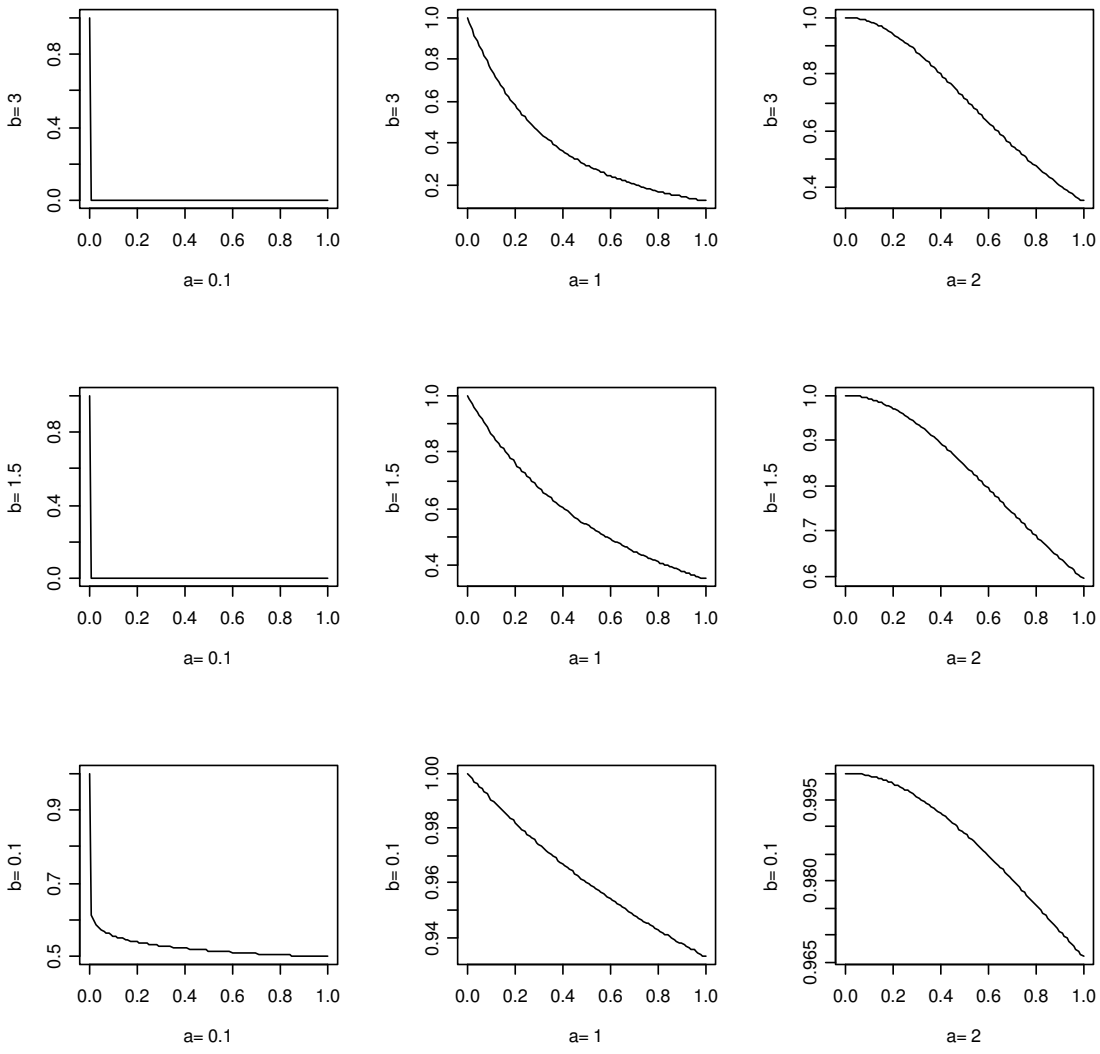

Figure M-8. Generalized Cauchy Cosine Models for $\rho = 0$.

M.5.4 Hyperbolic:

$$\varsigma(x) = \rho^2 + \left(1 - \rho^2\right) * c^{-b} \frac{(c^2 + x^2)^{0.5\,b}}{K_b(a * c)} * K_b(a\sqrt{c^2 + x^2}) \qquad \text{(M.5)}$$

The parameter constraints are {c>=0, a>0 and b>0}, or {c>0 , a>0 and b=0}, or {c>0 , a>=0, and b<0}. $K_b(x)$ denotes the modified Bessel function of the third kind of order *b.* Hyperbolic models are illustrated in Figure M-9 for $\rho = 0$ with parameter c=1 as black solid, c=2 as tan, and c=3 as thick dashed black curves.

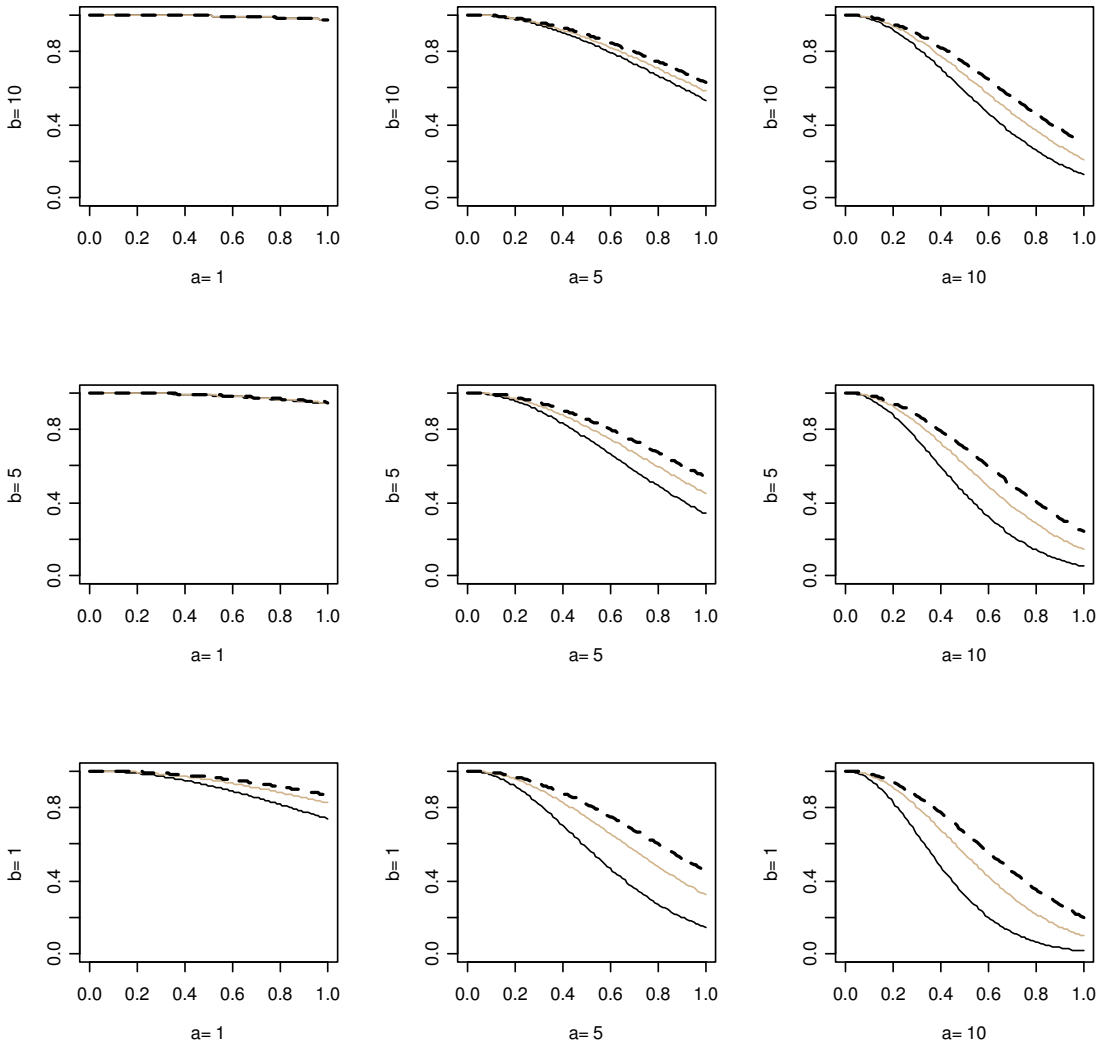

Figure M-9. Hyperbolic Cosine Models for $\rho = 0$.

M.5.5 Stable:

$$\varsigma(x) = \rho^2 + (1 - \rho^2) * \exp(-x^a),\ a \in (0,2] \tag{M.6}$$

Stable models are illustrated in Figure M-10 for $\rho = 0$ with parameter c=1 as black solid, c=2 as tan, and c=3 as thick dashed black curves.

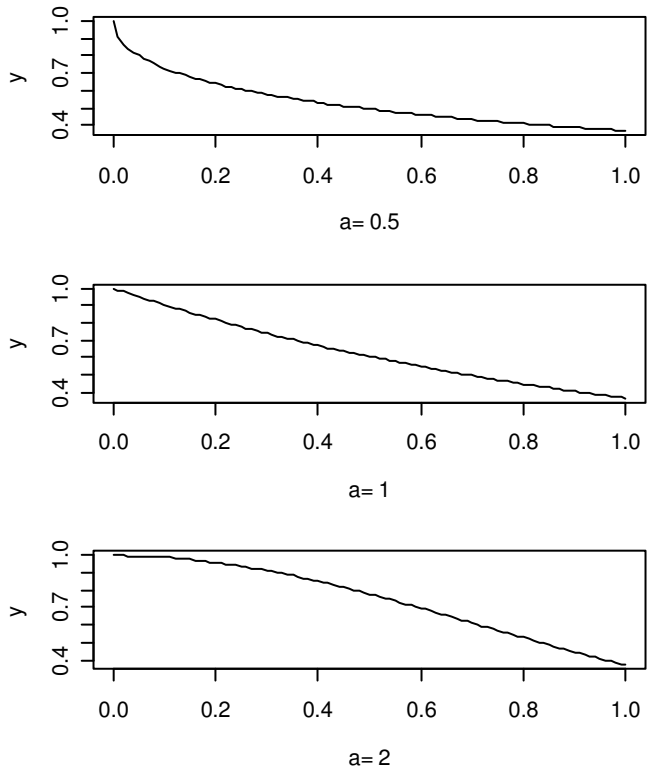

Figure M-10. Stable Cosine Models for $\rho = 0$.

M.6 Generalization of the Generation and Characterization of the Cosine Curves

The reader may choose from more than 30 GRF covariance models as provided by the R package Random Fields (Schlather 2001) function CovarianceFct. This function is embedded in the R code in Appendix K, Section K.14, MakeCosineData. MakeCosineData provides 5 circular distributions (cardioid, triangular, uniform, von Mises, wrapped Cauchy) with any valid value of parameter ρ or κ, depending on the distribution, and any range *r*. Additional circular distributions can be implemented either as a CDF table as described in Chapter 5, Section 5.3, 3), point 3, a) "Compute a table of the desired circular CDF ...", or as a closed form inverse CDF such as in 3), point 2 "For the triangular CRV ...", as appropriate.

The reader may use the code in Appendix L, Section L.10 as a template for generating a large series of cosine datasets. The dataset name references the circular distribution, the GRF covariance model, and the range *r*. For a more complicated example, U.GenCauchy_a_1.8_b_5.15_r_5 indicates that a uniform CRF was generated from a generalized Cauchy distribution with parameters $a = 1.8$, $b = 5.15$, and range $r = 5$. Note that these computations may take significant time, depending on the number of datasets, simulations, and observations per simulation.

The reader may use the code in Appendix L, Section L.12 as a template for plotting families of cosine curves produced.

Any of the covariance models of CovarianceFct may be used to fit a cosine curve because the code in Appendix K, Section K.15, FitCosineData, also uses the CovarianceFct function. The algorithm for achieving a sequence of decreasing local minima, as described in Section M.4, is tedious. The FitCosineData may be revised to implement other methods of fitting. To facilitate fitting, the inputs to MakeCosineData should be saved in the output object to be read by FitCosineData.

Appendix N

Additional Graphics for Circular Data

N.1 Summary Plots for Circular Data

Continuing from Chapter 1, Section 1.2, Figure N-1 (a) is a vector plot of the wind data. It shows magnitude (m/s) and direction. Quartiles of vector magnitude were colored, in order, blue, green, red, and violet, and the arrow heads of vectors were replaced with dots to eliminate coverage by the arrow heads. Figure N-1 (b) summarizes the circular data of Figure N-1 (a). The circular data plot is constructed similar to a histogram. The arc bin origin is 0°, bin width is 30°, and number of bins is 12. One dot for each observation is stacked on the outside of a circle at the center of its arc bin. The circular plot shows that the modal wind direction (arc bin with greatest number of observations) is toward about 105° (bin mid point) counterclockwise (CCW) from 0° E, or winds are blowing mostly from south-southeast to north-northwest.

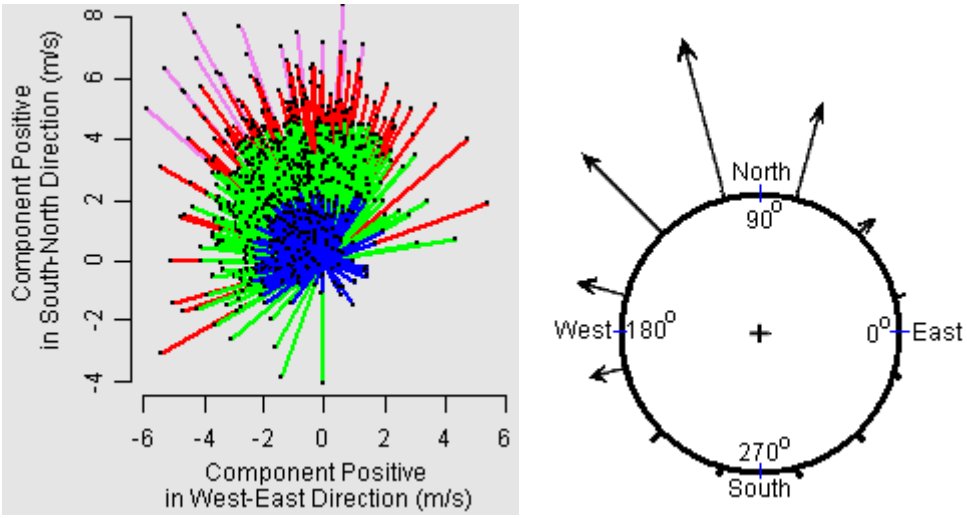

(a) (b)

Figure N-1. Summary Plots of the Ocean Wind Data. (a) Magnitude (length) and direction wind blows toward, (b) frequency (length) and direction.

N.2 Histograms for Circular Data

The histogram is a common method of summarizing numerical data. The data are grouped into intervals and the number of observations in each interval is counted. A rectangular bar of area proportional to the count in an interval is centered above the midpoint of the interval. The vertical axis of the histogram provides a scale for bar height. With the histogram, we can see the frequency with which data occur relative to the horizontal scale value, whether frequency is uniform over the range, or has some structure such as being concentrated at some value on the horizontal scale. The histogram for circular data is constructed similarly. An arc bin origin (e.g., 0°) and arc bin width (e.g., 5°, 10°, 20°, or 30°) are selected, and the data are binned and counted. The next step is to wrap the horizontal axis of the histogram around a unit circle. The bars are aligned with the circle center and arc interval midpoint, plotted on the outside of the circle, and have length or area proportional to count or relative frequency. Vector magnitude is ignored.

The circular histograms in Figure N-2 summarize the same data as shown in Figure N-1 with the same bin origin of 0° and bin width of 30°. Figure N-2 (a) shows a rose plot (Florence Nightingale) of wind direction. The angle of the wedge is the bin width and the area of a wedge is proportional to the bin count. Figure N-2 (b) shows a circular histogram with a bar area corresponding to bin count. Figure N-2 (c) unwraps the circular histogram of Figure N-2 (b) onto a linear scale and repeats one period. The additional period facilitates visual extraction of period, counting of modes, and prevents breakup of features occurring near the cross over point of 360° (0°). Additionally, Figures N-2 (a) to (c) show the estimated mean (vector resultant direction) of 106.3° and the 95% confidence interval (104.8°,107.8°) for the mean. This confidence interval is based on the von Mises distribution (Fisher 1993, pp. 88-89). In Figures N-2 (a) and (b),

the mean direction is indicated by a thick black radial line from the circle center with the confidence interval indicated by a black arc slightly outside the large circle. In Figure N-2 (c), the mean is indicated by a black solid vertical line enclosed in confidence limits displayed as vertical dashed lines.

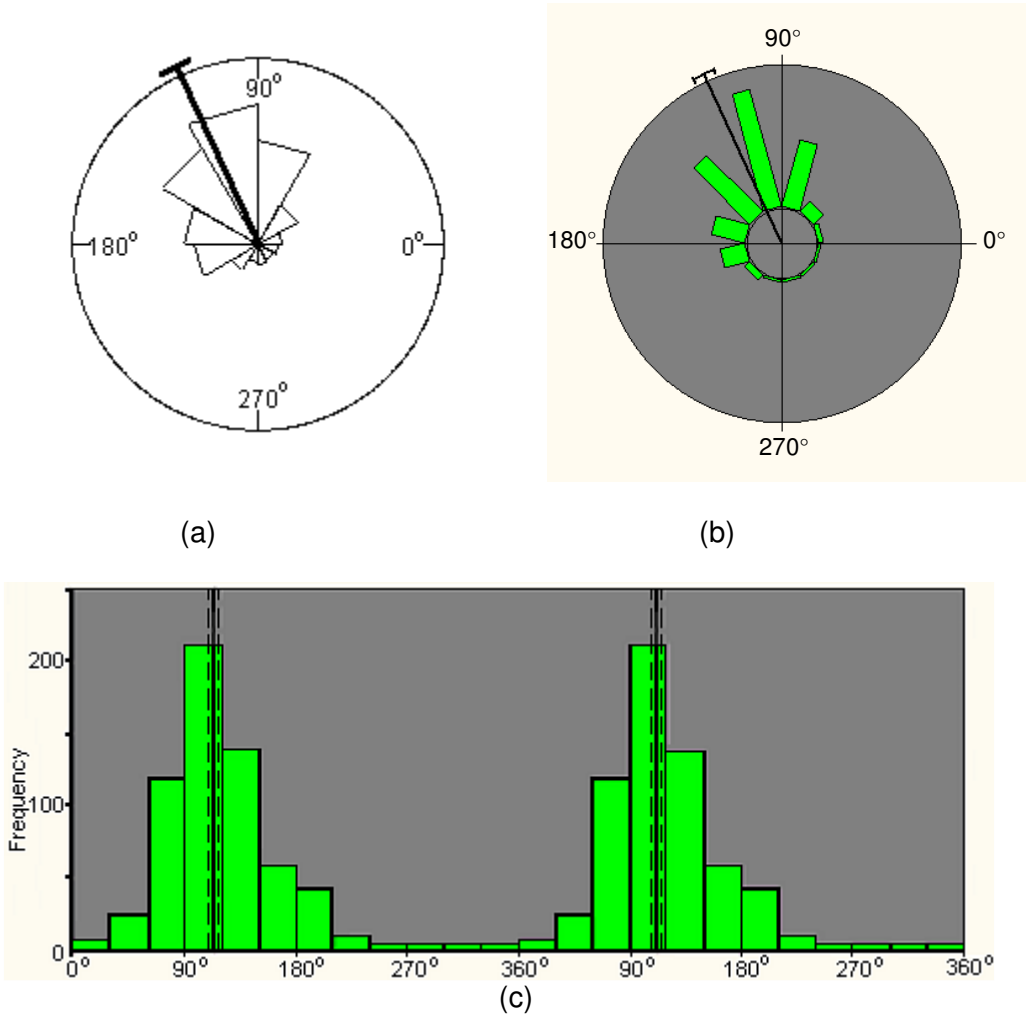

Figure N-2. Circular Histograms of the Ocean Wind Data. (a) Rose plot, (b) circular histogram, and (c) linearized circular histogram summarize circular data. (c) repeats the histogram to facilitate visual extraction of period, counting of modes, and prevent breakup of features occurring near the cross over point of 360°.

N.3 Nonparametric Density Plots for Circular Data

The kernel density estimates in Figure N-3 are based on the same data as was used in Figures N-1 and N-2. Circular histograms of Figure N-2, like histograms for linear variables, can distort the structural information in the sample about the number, locations, and sizes of modes through an arbitrary choice of bin origin and bin width. The nonparametric smoothed density estimate replaces the bin edge and origin decisions with an easier smoothing band width decision. In nonparametric smoothing, a symmetric unimodal function is centered on each observation. It effectively spreads out the mass of an observation with maximum value at the location of the observation, mimicking the stochastic process where the observation is an instance of a random direction and could have occurred at other locations in the neighborhood of the observed direction. Increasing the bandwidth increases smoothness and decreases noise. Decreasing bandwidth exposes more structural detail and noise. The smoothed histograms of Figure N-3 implement the kernel density method for a CRV given in Fisher (1993, pp. 26-27).

Figure N-3 (a) plots the estimated data density on the outside of a unit circle. The density at a given angle (direction) is the radial distance between the red and the grey curves at the given angle. Figure N-3 (b) shows the density of Figure N-3 (a) unwrapped onto a linear scale with an extra period. Like the linearized circular histogram in Figure N-2 (c), the extra period eliminates the breakup of features at the cross over point of 360° and makes it easier to assess structure. This density estimation method indicates that there is one mode at about 105° CCW from 0° E.

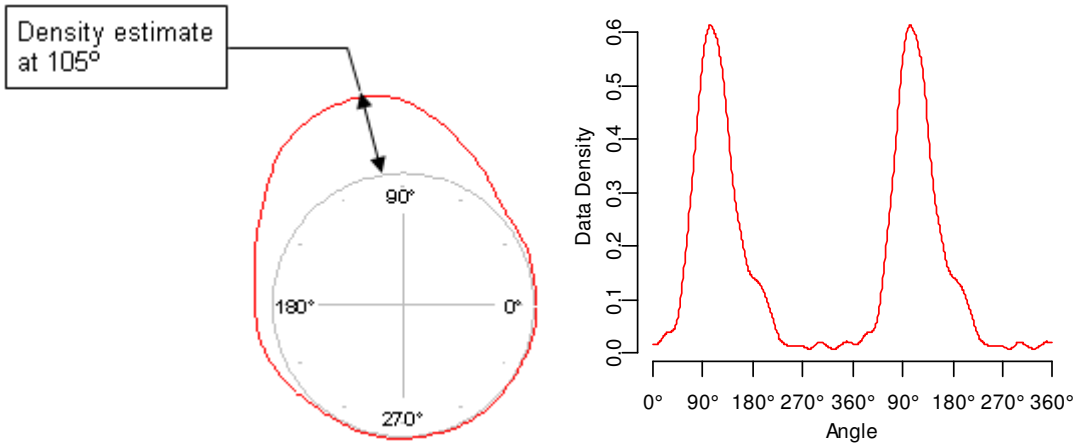

(a) (b)

Figure N-3. Kernel Density Plots of the Ocean Wind Data. (a) Circular, (b) linear with extra period. There is one mode at about 105° CCW from 0° E.

N.4 New Cylindrical Plot of the Circular Probability Density

Figure N-3 (a) is an example of the traditional method of plotting the probability density function (PDF) of a CRV with radius equal to 1.0 + density with density depending on direction. Figure N-4 shows a new method for displaying the circular PDF. The PDF is drawn as a cylinder of unit radius with height of the cylinder at an angle equal to the probability density at the angle. Note that, as stated in Chapter 1, Section 1.1, the unit of angular measurement is radians because PDFs generally contain trigonometric functions that require angles in radian units. This method maintains the requirement that the area between the PDF and circular scale must equal 1.0 over the support. In general, the traditional circular display of the PDF does not integrate to one as does the linear display. For a circular uniform distribution with density $1/(2\pi)$ on $[0,2\pi)$ or $[-\pi,+\pi)$ radians, we would draw circles of unit radius and radius $1+1/(2\pi)$. The area between the outer circle and the unit circle representing the total probability

should equal 1.0, but it is actually $1+1/(4\pi)$. However, the traditional display is easy to draw, intuitive, and is widely used.

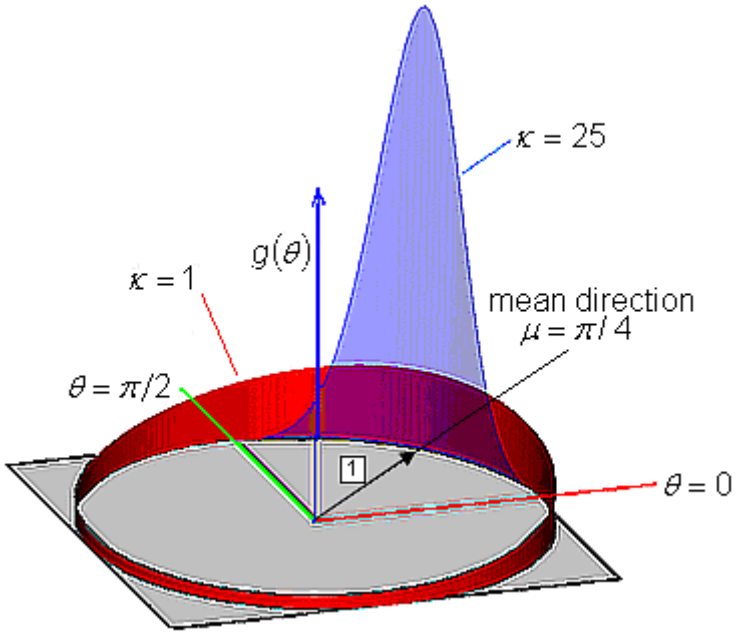

Figure N-4. New Cylindrical Plot of PDFs of von Mises Probability Densities. Direction is expressed in radian units. The distribution with $\kappa = 25$ is more concentrated and less variable than the distribution with $\kappa = 1$.

Figure N-4 shows two von Mises probability densities with concentration parameters $\kappa = 1, 25$ (see Chapter 3, Table 3-1). The concentration parameter κ is a measure of variability for the von Mises distribution equal to ½ the log of the ratio of maximum density to the density at the opposite direction. Hence, large values correspond to distributions of low variability and concentrated about the mean.